– For internal NASA use only –

Lunar Meteoroid Ejecta Engineering Model

Anthony M. DeStefano
NASA MSFC EV44

February 25, 2022

Contents

1 Executive Summary **1**

2 Lunar Regolith Properties **1**
2.1 Porosity . . . 1
2.2 Density . . . 1
2.3 Strength . . . 4
2.4 Particle Size Distribution . . . 6
2.5 Scaling Law Parameters . . . 10

3 Primary Flux Environment **11**
3.1 Space-Time Dependence of Environment . . . 11
3.1.1 Ephemeris Definition . . . 13
3.1.2 Selenographic Extent . . . 13
3.2 Sporadic Meteoroid Complex . . . 13
3.2.1 Angular Distribution . . . 13
3.2.2 Density Distribution . . . 13
3.2.3 Mass Distribution . . . 13
3.3 Near-Earth Objects . . . 13
3.3.1 Speed Distribution . . . 13
3.3.2 Mass Distribution . . . 13
3.4 Meteoroid Showers . . . 13

4 Secondary Flux Environment **13**
4.1 Ejecta Distribution . . . 13
4.1.1 Speed Distribution . . . 13
4.1.2 Zenith Distribution . . . 13
4.1.3 Azimuth Distribution . . . 13
4.2 Mass/Particle Size Distribution . . . 13

4.3 Orbital Mechanics . . . 13
4.3.1 Crater on Surface to Observer at Surface . . . 13
4.3.2 Crater on Surface to Observer at or above Surface . . . 13
4.4 Selenographic Distance & Bearing . . . 13

5 Scaling Laws **13**
5.1 Crater Size – Strength & Gravity Regime . . . 13
5.2 Minimum & Maximum Ejected Speed . . . 13
5.3 Maximum Ejected Particle Mass . . . 13
5.4 Mass Ejected from Crater . . . 13

References **14**

List of Figures

1 A comparison of the regolith bulk density for a certain depth depth (blue), the depth-averaged bulk density (orange), and the volume-averaged bulk density (green). See also, Figure 9.16 of the Lunar Sourcebook [*Heiken et al.*, 1991]. . . . 2
2 Relative error of using the density at a certain depth (blue) and using the depth-weighted average (orange) of the regolith bulk density. . . . 4
3 The range of regolith shear strength as a function of depth below the lunar surface taken from Figure 9.26 of the Lunar Sourcebook. The average shear strength is also calculated (green). Points that are extrapolated beyond what is available are shown by the dashed lines. The volume-averaged shear strength (red) assumes a parabolic-shaped crater of depth z. . . . 5
4 Geotechnical particle size distribution: middle curve showing the average distribution; left-hand and right-hand curves showing ± 1 standard deviation [*Carrier III*, 2003]. Note, that the percent passing is normalized by mass and not particle number [see *Carrier*, 1973]. . . . 6
5 Plots of the mass-weighted and number-weighted CDFs and PDFs derived from *Carrier III* [2003]. Top left: the digitized data from Figure 1 of *Carrier III* [2003] is shown with the log-normal distribution fit. Top right: The mass-weighted PDF * dx is shown to dictate what particle size dominates the contribution of mass. Bottom left: The number-weighted CDF showing number of particles in 1 kg of regolith greater than a size x. Bottom right: The number-weighted PDF is shown in units of mm^{-1}. . . 8
6 Fluxes at the meridional plane (as a function of impact speed and angle from the horizon) of the low density population (a) and (b), and the high density population (c) and (d) impacting the Moon at the equator (a) and (c), and the north/south pole (b) and (d). . . . 11

List of Tables

1 Porosity for various depths. 1
2 The change of the shear strength of the lunar soil with depth. 5
3 Digitized data points from Figure 4, see *Carrier III* [2003]. 7
4 Summary of constants used in the *Housen and Holsapple* [2011] ejecta model. 10

1 Executive Summary

2 Lunar Regolith Properties

2.1 Porosity

The lunar regolith porosity is related to the amount of free space between individual grains. The greater the porosity, the more void space is present. Table 3.4.2.3.4-1 of the DSNE gives values of the porosity as a function of depth down to 60 cm derived from Apollo core measurements (copied from Table 9.5 of the Lunar Sourcebook, *Heiken et al.* [1991]) and shown here in Table 1.

Table 1: Porosity for various depths.

Depth Range (cm)	Average Porosity, n (%)
$0-15$	52 ± 2
$0-30$	49 ± 2
$30-60$	44 ± 2
$0-60$	46 ± 2

2.2 Density

The bulk density (ρ) of the lunar regolith is defined as the mass of material in a given volume, which relates the particle density (ρ_p) and porosity (n) to the bulk density as (see Section 3.4.2.3.1 of the DSNE or Chapter 9 of the Lunar Sourcebook)

$$\rho = \rho_p(1-n). \tag{2.1}$$

The DSNE suggests using $\rho_p = 3.1$ g/cm^3 for the average particle density over the entire Moon. Otherwise, the typical highlands particle density is $\rho_p = 2.75\pm0.1$ g/cm^3 whereas the typical mare particle density is $\rho_p = 3.35\pm0.1$ g/cm^3.

The bulk density[1] as a function of depth, fit to Apollo data, is given by

$$\rho(z) = 1.92\frac{z+12.2}{z+18}, \tag{2.2}$$

where z is the depth in cm and ρ is in units of g/cm^3. At the surface ($z=0$), the density is 1.30 g/cm^3, and increases to 1.92 g/cm^3 for large depths. This expression is fairly reasonable down to 3 m (the limit reached by Apollo drill core samples). In order to get an up-to-depth average of the bulk density, take

$$\rho_{avg,depth}(z) = \frac{1}{z}\int_0^z dz'\rho(z'), \tag{2.3}$$

[1]Follows the average particle density of 3.1 g/cm^3 for all depths with a porosity depth dependence following Table 1, see the *porosity of lunar soil* paragraph on page 492 in the Lunar Sourcebook.

which gives (compare with the equation for d_m on page 494 of the Lunar Sourcebook)

$$\rho_{avg,depth}(z) = 1.92\left[1 - \frac{5.8\ln\left(\frac{z+18}{18}\right)}{z}\right]. \tag{2.4}$$

For example, the average bulk density of the regolith with a depth range of $0 - 60$ cm would be $\rho_{avg,depth}(60)$ = 1.65 g/cm^3.

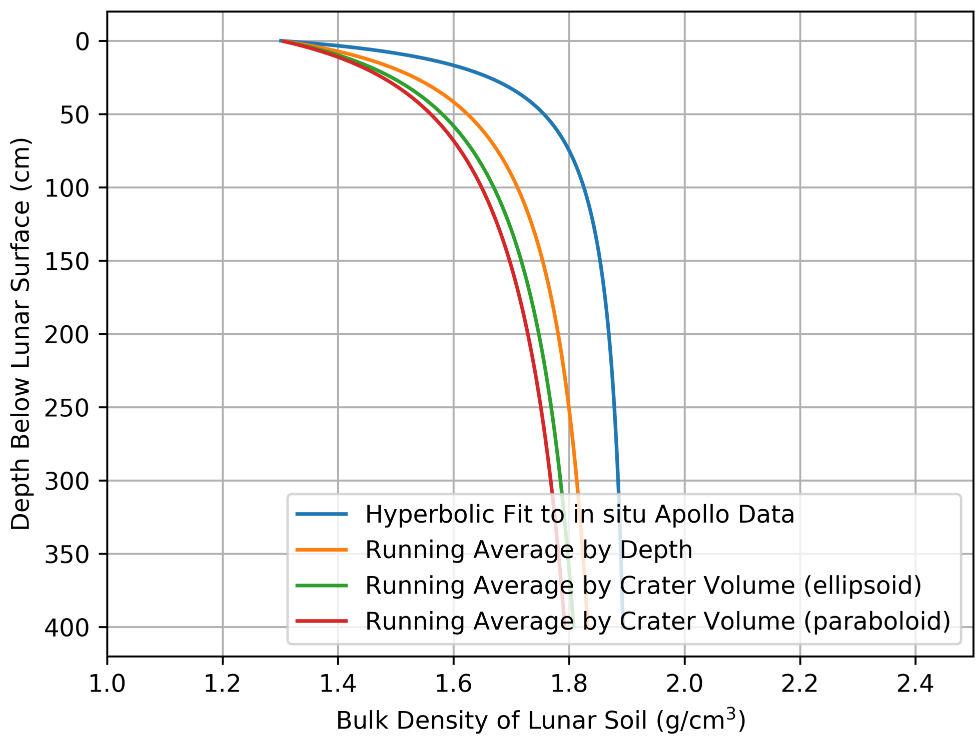

Figure 1: A comparison of the regolith bulk density for a certain depth depth (blue), the depth-averaged bulk density (orange), and the volume-averaged bulk density (green). See also, Figure 9.16 of the Lunar Sourcebook [*Heiken et al.*, 1991].

For a higher-fidelity estimate of the average bulk density sampled by the crater, a volume-average can be used instead of a depth-average, given by

$$\rho_{avg,volume}(z) = \frac{\int dV\,\rho(z')}{\int dV}. \tag{2.5}$$

Expanding the integral in a cylindrical coordinate system and assuming an ellipsoidal crater shape, Equation (2.5) becomes

$$\rho_{avg,ellipsoid}(z) = \frac{\int_0^z \int_0^{R\sqrt{1-z'^2/z^2}} \int_0^{2\pi} d\phi r dr dz' \rho(z')}{\int_0^z \int_0^{R\sqrt{1-z'^2/z^2}} \int_0^{2\pi} d\phi r dr dz'} \tag{2.6}$$

$$= \frac{1.92}{4z^3}\left[z(6ab - 6b^2 - 3az + 3bz + 4z^2) + 6(a-b)(b^2 - z^2)\ln\left(\frac{b}{z+b}\right)\right], \tag{2.7}$$

for the volume-averaged density in g/cm^3 with z in cm, where $a = 12.2$ and $b = 18$. Following the example from earlier, the average bulk density of the regolith with a depth range of $0 - 60$ cm would be $\rho_{avg,ellipsoid}(60) = 1.60$ g/cm^3, which is $\sim 3\%$ less than $\rho_{avg,depth}(60) = 1.65$ g/cm^3.

On the other hand, if a paraboloid crater shape is assumed, Equation (2.5) becomes

$$\rho_{avg,paraboloid}(z) = \frac{\int_0^z \int_0^{R\sqrt{1-z'/z}} \int_0^{2\pi} d\phi r dr dz' \rho(z')}{\int_0^z \int_0^{R\sqrt{1-z'/z}} \int_0^{2\pi} d\phi r dr dz'} \tag{2.8}$$

$$= \frac{1.92}{z/2}\left[b - a + \frac{z}{2} - \frac{(a-b)(b+z)\ln\left(\frac{b}{z+b}\right)}{z}\right], \tag{2.9}$$

using the same values for a and b as before. Again, with the prior example, the average bulk density of the regolith with a depth range of $0 - 60$ cm would be $\rho_{avg,paraboloid}(60)$ = 1.58 g/cm^3, which is $\sim 4\%$ less than $\rho_{avg,depth}(60) = 1.65$ g/cm^3, see Figure 2. The expression given in Equation (2.9) is useful for computing the ejected mass from a crater[2], given a crater depth z.

The expressions for the regolith density at a certain depth z, weighted by depth, and weighted by crater volume (ellipsoid and paraboloid) are given by Equations (2.2), (2.4), and (2.7), (2.9), respectively, are compared in Figure 1. The crater volume is approximated as a half-ellipsoid with two of the dimensions scaled by the crater radius R and one dimension scaled by the crater depth z, sliced such that the half-ellipsoid is symmetric about the surface normal for Equation (2.7). On the other hand, a paraboloid-shaped crater is used for Equation (2.9). For a given crater, more of the volume is near the surface so that more weight is given by bulk densities that originate near the surface. In contrast, the depth-averaged bulk density takes the bulk density at each depth equally. This results in the volume-averaged bulk density to be slightly less than the depth-averaged bulk density, as shown in Figure 1. In addition, comparing an ellipsoidal crater vs. a parabolic crater, the parabolic crater (typically used in literature, see *Singer et al.* [2020]) exhibits the softest increase of the average bulk density as a function of depth.

[2] In an iterative fashion, since the crater radius depends on the regolith density.

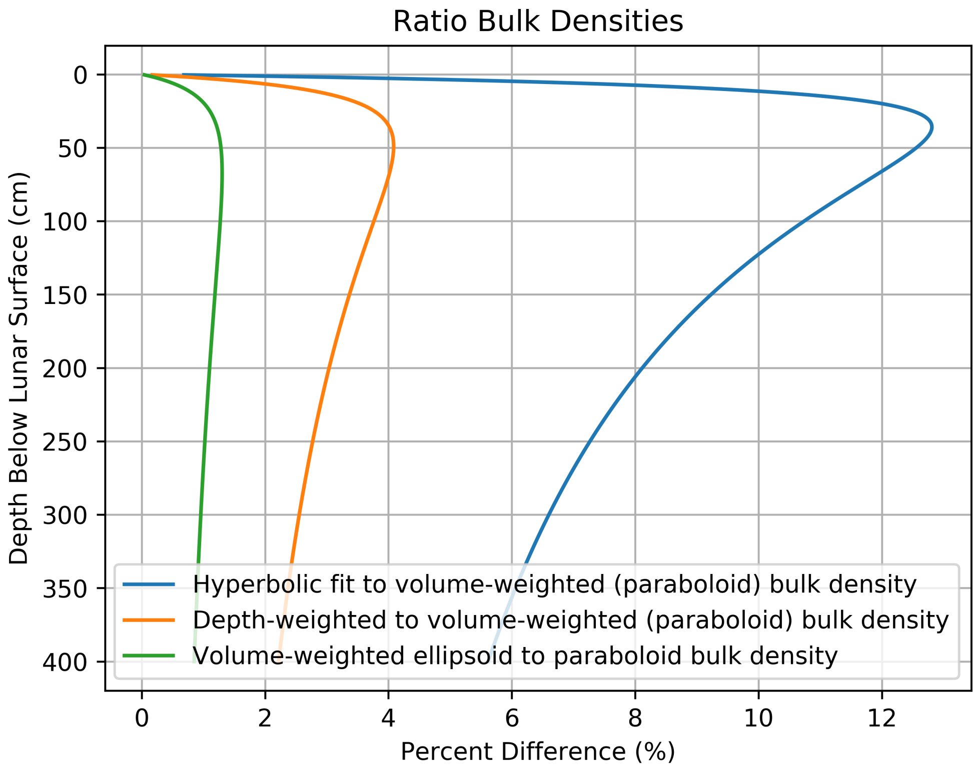

Figure 2: Relative error of using the density at a certain depth (blue) and using the depth-weighted average (orange) of the regolith bulk density.

2.3 Strength

The strength of the regolith can be measured in different ways, depending on the use. In the case of modeling impacts, the shear strength of loose regolith and tensile strength of solid rock can be used. The top 10 m or so consists of fine-grained material called regolith. From 10 m to about 2 km is the large scale ejecta that is course grained and ballistically transported (Fig 4.22 of the Lunar Sourcebook, *Heiken et al.* [1991]). All of the impacts studied in this model will create craters less than 2 km, so it is expected that the shear strength will be used for the loose regolith and large scale ejecta material.

The shear strength of the lunar soil increases with the depth. As an example, both Figure 9.26 of the Lunar Sourcebook, reproduced in Figure 3, and Table 12 of *Slyuta* [2014] depict this characteristic, shown in Table 2.

The average shear strength (green curve) in Figure 3 can be expressed by the

Table 2: The change of the shear strength of the lunar soil with depth.

Depth (cm)	Shear strength (kPa)
5	$0.1 - 2.5$
50	$1 - 3.5$
100	$2 - 4$
200	$4 - 8$

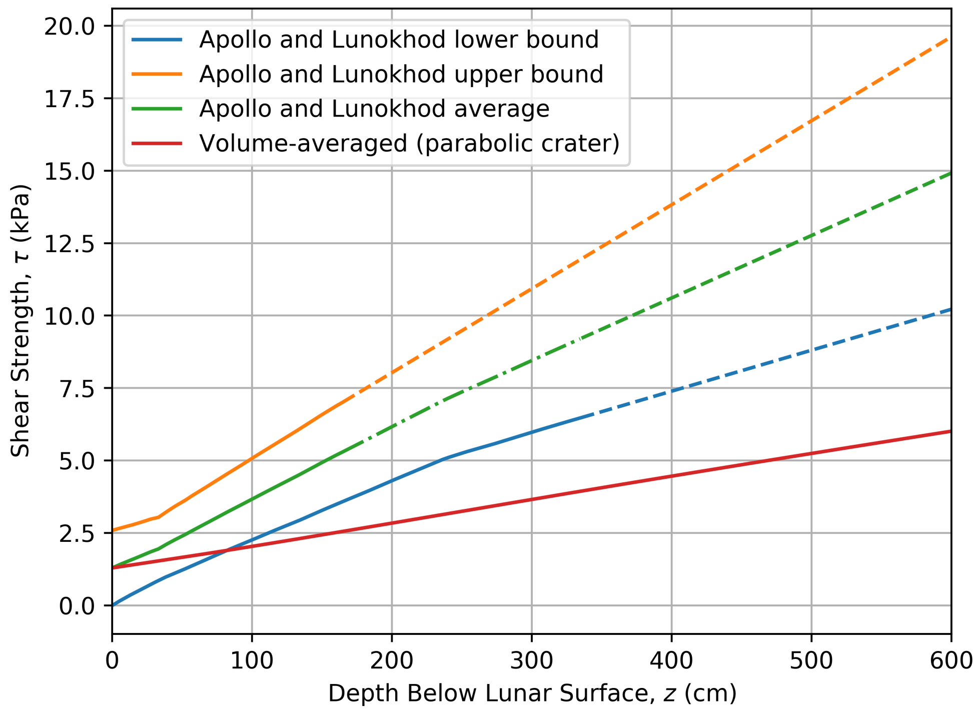

Figure 3: The range of regolith shear strength as a function of depth below the lunar surface taken from Figure 9.26 of the Lunar Sourcebook. The average shear strength is also calculated (green). Points that are extrapolated beyond what is available are shown by the dashed lines. The volume-averaged shear strength (red) assumes a parabolic-shaped crater of depth z.

piece-wise form

$$\tau(z) = \begin{cases} \frac{z}{45.55} + 1.288, & 0 \leqslant z < 50 \text{ cm} \\ \frac{z}{40.21} + 1.144, & 50 \text{ cm} \leqslant z < 250 \text{ cm} \\ \frac{z}{46.06} + 1.942, & z \geqslant 250 \text{ cm} \end{cases} . \tag{2.10}$$

Assuming the crater has a parabolic shape and that the effective shear strength is the volume-average (similar approach to Equation (2.5)), Equation (2.10) becomes (as shown by the red curve in Figure 3)

$$\tau(z) = \begin{cases} \frac{z}{136.65} + 1.288, \ 0 \leqslant z < 50 \text{ cm} \\ \frac{z}{120.63} + 1.144 + \frac{7.163}{z} - \frac{118.33}{z^2}, \ 50 \text{ cm} \leqslant z < 250 \text{ cm} \\ \frac{z}{138.18} + 1.942 - \frac{194.81}{z} + \frac{16902}{z^2}, \ z \geqslant 250 \text{ cm} \end{cases} . \tag{2.11}$$

2.4 Particle Size Distribution

The cumulative distribution function (CDF) of the regolith particle sizes[3] are fit to several Apollo samples, as shown in Figure 4. During an impact, the particle size distribution may become modified and are organized depending on the ejected speed (see Section 4.2). However, the unmodified regolith size distribution is given in this section for reference. The digitized data from Figure 4 is shown in Table 3.

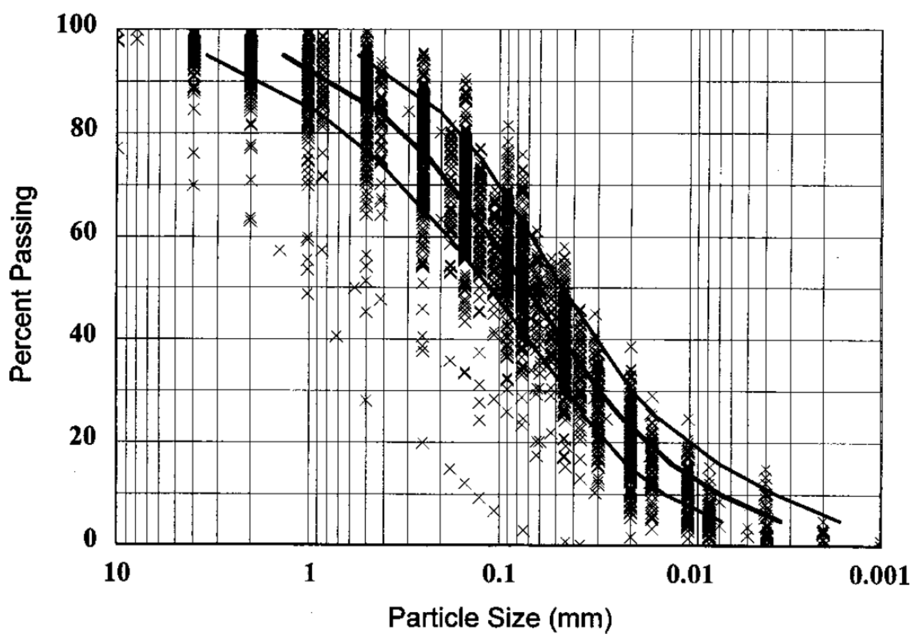

Figure 4: Geotechnical particle size distribution: middle curve showing the average distribution; left-hand and right-hand curves showing ± 1 standard deviation [*Carrier III*, 2003]. Note, that the percent passing is normalized by mass and not particle number [see *Carrier*, 1973].

In *Carrier III* [2003], they specifically call out that the mass-weighted CDF can be modeled by a log-normal distribution, so this assumption is made below. By definition,

[3] In the context here, particle size is defined as the particle diameter of a spherical-shaped particle. Other sections may define size by the radius.

Table 3: Digitized data points from Figure 4, see *Carrier III* [2003].

Particle Diameter (mm)	Cumulative Percent by Mass
0.003380248352585	5.17682028091534
0.003794441295246	6.09401642297017
0.00451292465605	7.2776812909626
0.0053674729594	8.4354410787182
0.006383732464611	9.71063723021409
0.007592176031253	11.2086170717467
0.009029116435596	12.9190185712213
0.010737989052827	14.65100763756
0.012769865152208	16.6247774527757
0.015185144104918	19.116648872728
0.018057261192048	21.6025237463292
0.02136872870221	24.2948870610798
0.025044648784976	27.0334149904509
0.029494364580794	29.8741284657866
0.033098954040892	32.8807708128992
0.037145453042138	35.6150479687852
0.042499223173782	38.2089250804786
0.048155933590968	41.1181012805662
0.054042887826956	43.8970091889745
0.060942690951498	46.6685810695819
0.068720899309714	49.7075873197331
0.077869796000019	52.4248808897808
0.087812953450079	55.0874612212659
0.098550426314892	57.6779504306929
0.112206724061769	60.6265864834011
0.127759476997186	63.3415731364729
0.145465039759366	66.2037864789212
0.168035843630453	69.131911259623
0.19411176280305	71.9484525505802
0.222083419318477	74.7285290349147
0.259044020108005	77.2129935126797
0.30803890584547	79.7150699642405
0.366294873918129	82.3305792671413
0.435590409221425	84.5720349114709
0.518029785192508	86.3256115446736
0.616085725364177	87.9108051563369
0.732705596850257	89.4631856663669
0.871382022892136	91.1718601604924
1.03629488039837	92.9535006306183
1.23245384670266	94.5235829454768

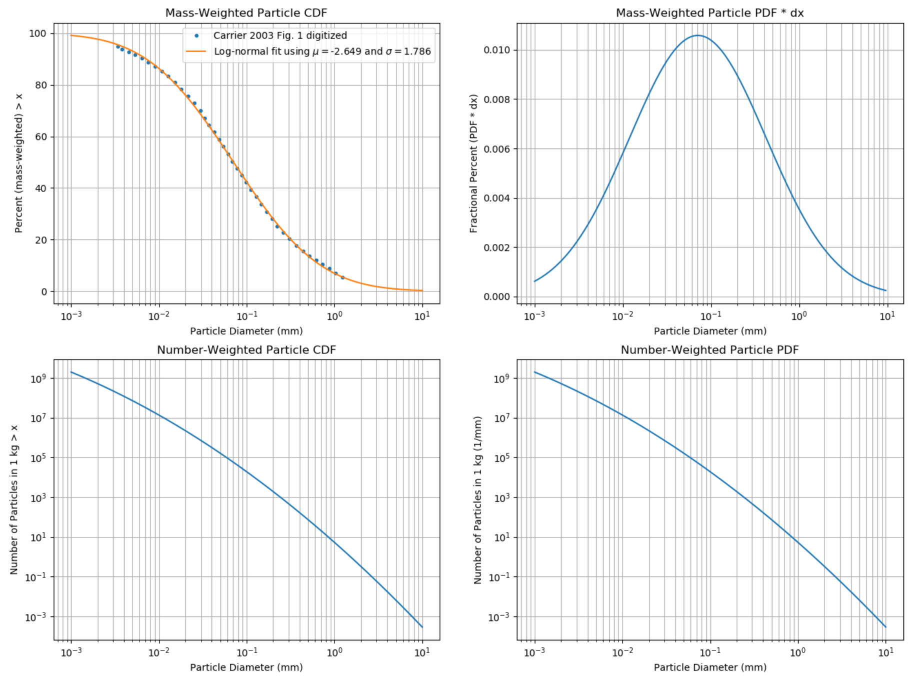

Figure 5: Plots of the mass-weighted and number-weighted CDFs and PDFs derived from *Carrier III* [2003]. Top left: the digitized data from Figure 1 of *Carrier III* [2003] is shown with the log-normal distribution fit. Top right: The mass-weighted PDF * dx is shown to dictate what particle size dominates the contribution of mass. Bottom left: The number-weighted CDF showing number of particles in 1 kg of regolith greater than a size x. Bottom right: The number-weighted PDF is shown in units of mm^{-1}.

a log-normal distribution is given by

$$F_{\text{kg}}(>x) = 1 - F(<x)_{\text{kg}} = \frac{1}{2}\left[1 - \text{erf}\left(\frac{\ln x - \mu}{\sqrt{2}\sigma}\right)\right], \tag{2.12}$$

where x is the particle diameter size in units of mm, μ is the expected value of $\ln x$, and σ is the standard deviation of $\ln x$.

The PDF is then given by

$$f_{\text{kg}}(x) = \frac{1}{\sigma\sqrt{2\pi}}\frac{1}{x}\exp\left[-\frac{(\ln x - \mu)^2}{2\sigma^2}\right]. \tag{2.13}$$

In order to have the number-weighted PDF and CDF, we begin with $f_{\text{kg}}(x)$ and divide by the mass of a given particle size (diameter), [e.g., Equation (7) of *Koschny* *and Grün*, 2001]

$$m(x) = \frac{\pi}{6}\rho x^3, \tag{2.14}$$

so that we have (assuming F_{kg} represents the CDF for 1 kg of regolith)

$$f_{\text{number}}(x) = \frac{f_{\text{kg}}(x)}{m(x)} = \frac{6}{\pi\rho}\frac{1\text{kg}}{1\text{mm}^3}\frac{1}{\sigma\sqrt{2\pi}}\frac{1}{x^4}\exp\left[-\frac{(\ln x-\mu)^2}{2\sigma^2}\right], \tag{2.15}$$

for the number-weighted PDF. To arrive at the number-weighted CFD, integration over $f_{\text{number}}(x)$ is done such that

$$F_{\text{number}}(>x) = \int_x^\infty dx' f_{\text{number}}(x'). \tag{2.16}$$

Solving the integral, the number-weighted CDF is given by

$$F_{\text{number}}(>x) = \frac{6}{\pi\rho}\frac{1\text{kg}}{1\text{mm}^3}\frac{1}{\sigma\sqrt{2\pi}}\left[1-\text{erf}\left(\frac{\ln x-\mu+3\sigma^2}{\sqrt{2}\sigma}\right)\right]\exp\left(-3\mu+\frac{9\sigma^2}{2}\right), \tag{2.17}$$

which is the number of particles of diameter x or greater in 1 kg of regolith. For $F_{\text{number}}(<x)$, flip the minus sign to a plus sign on the error function. Note that $\text{erfc}(x) = 1-\text{erf}(x)$.

Fitting the mass-weighted CDF $F(<x)$ to Figure 4, the following parameters are obtained:

$$\mu = -2.649, \tag{2.18}$$
$$\sigma = 1.786, \tag{2.19}$$

where the mean, median, and mode particle size (weighted by mass) is

$$x_{\text{mean}} = \exp\left(\mu+\frac{\sigma^2}{2}\right) = 34.8\mu\text{m}, \tag{2.20}$$
$$x_{\text{median}} = \exp(\mu) = 7.07\mu\text{m}, \tag{2.21}$$
$$x_{\text{mode}} = \exp\left(\mu-\sigma^2\right) = 0.291\mu\text{m}. \tag{2.22}$$

If the mean, median, and mode particle size weighted by number are needed, then the modified parameters are

$$\mu^\star = \mu - 3\sigma^2 = -12.22, \tag{2.23}$$
$$\sigma^\star = \sigma = 1.786, \tag{2.24}$$

giving the following (now weighted by number):

$$x^\star_{\text{mean}} = \exp\left(\mu^\star+\frac{\sigma^{\star 2}}{2}\right) = 2.43\text{ nm}, \tag{2.25}$$
$$x^\star_{\text{median}} = \exp(\mu^\star) = 0.494\text{ nm}, \tag{2.26}$$
$$x^\star_{\text{mode}} = \exp\left(\mu^\star-\sigma^{\star 2}\right) = 0.0203\text{ nm}. \tag{2.27}$$

Note that these set of averages are outside the range of the data provided in *Carrier III* [2003] and are only valid if the log-normal distribution holds for these very small particles. This regime is on the order of several atomic nuclei large.

As an example, if the number of particles greater than 1 μg per 1 kg of regolith are needed, then use Equation (2.17) (assuming a regolith density of ρ = 3.1 g / cm^3 such that $x(1\mu\text{g}) = 8.509\mu\text{m}$)

$$F_{\text{number}}(> x = 8.509\mu\text{m}) = 3.146 \times 10^7 \text{ \# of particles per 1 kg of regolith.} \quad (2.28)$$

2.5 Scaling Law Parameters

In the meteoroid ejecta model described in this document, the scaling laws from *Housen and Holsapple* [2011] are employed. In this section, the parameters of various material types used in fits to the scaling laws are summarized. The specific scaling law equations are discussed in Section 5.

The various sets of parameters for different target materials are given in Table 3 of *Housen and Holsapple* [2011] with most of them copied here in Table 4, with undefined values filled in that are best represented by either solid, semi-solid, or fine material where applicable. If a material has zero strength, the crater scaling is automatically in the gravity regime and there is no strength regime (and no need for H_2 to be defined).

Table 4: Summary of constants used in the *Housen and Holsapple* [2011] ejecta model.

Curve no.	C1	C2	C3	C4	C5	C6	C7	C8
Target	Water	Rock	WCB	Sand	Sand	GMS	SFA	PS
Porosity	~ 0	~ 0	20%	$35 \pm 5\%$	$35 \pm 5\%$	36%	45%	60%
μ	0.55	0.55	0.46	0.41	0.41	0.45	0.4	0.35
C_1	1.5	1.5	0.18	0.55	0.55	1.0	0.55	0.6
k	0.2	0.3	0.3	0.3	0.3	0.5	0.3	0.32
H_1	0.68	0.68^{*1}	0.5^{*2}	0.59	0.59	0.8	0.59^{*3}	0.59^{*3}
H_2	–	1.2	0.38	–	–	–	0.4	0.81
$n_{2,G}$	1.5	1.5	1.3^{*3}	1.3	1.3	1.3	1.2^{*2}	1.2^{*2}
p	0.5	0.5	0.3	0.3	0.3	0.3	0.3	0.2
Y (MPa)	0	30	0.45	0	0	0	4×10^{-3}	2×10^{-3}

Note: WCB = weakly cemented basalt, GMS = glass micro-spheres, PS = perlite/sand mixture, SFA = sand/fly ash. All cases shown in this table used: $\nu = 0.4$, $n_1 = 1.2$, $n_{2,S} = 1$, $g = 9.81$ m/s^2.
$*1$ from water, $*2$ no value given, $*3$ from sand.

The average regolith porosity from $0 - 60$ cm is $46 \pm 2\%$ (see Table 1), so the set of parameters that define SFA (sand/fly ash) are adopted. For a higher fidelity strength, Equation (2.11) can be used instead of $Y = 4$ kPa.

3 Primary Flux Environment

3.1 Space-Time Dependence of Environment

The primary flux of sporadic meteoroids onto the surface of the Moon changes depending on the selenographic location on the Moon. Because of this effect, ephemeris data[4] was generated for different latitudes and longitudes on the Moon in 5-degree increments from pole to pole, and in 90-degree increments in longitude. A time frame of 19 years was chosen, or a Metonic cycle, which takes into account many different Sun-Earth-Moon geometries.

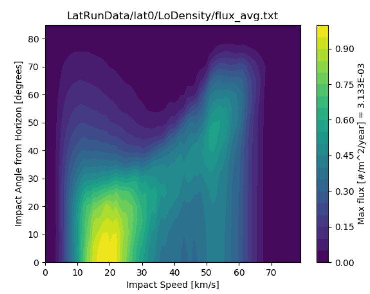

(a) Low density population impacting at the equator.

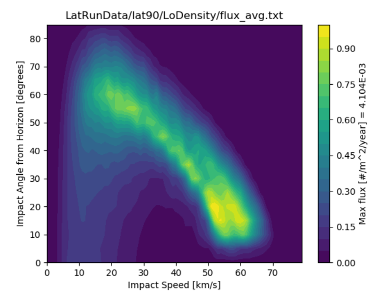

(b) Low density population impacting at the north pole.

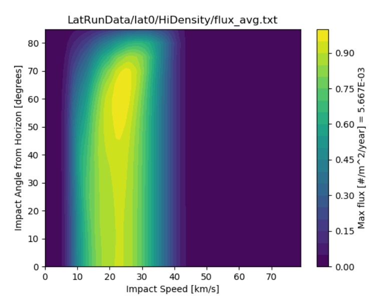

(c) High density population impacting at the equator.

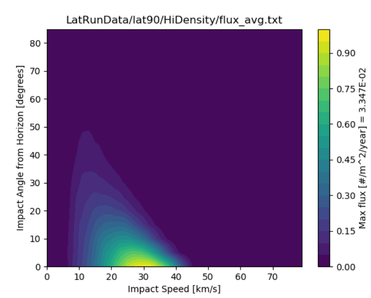

(d) High density population impacting at the north pole.

Figure 6: Fluxes at the meridional plane (as a function of impact speed and angle from the horizon) of the low density population (a) and (b), and the high density population (c) and (d) impacting the Moon at the equator (a) and (c), and the north/south pole (b) and (d).

As an example, in Figure 6, the speed-angle flux distribution is shown at the equator and at the poles for the low and high density MEM populations. Note that the fluxes in the northern and southern hemispheres are symmetric about the equator. It can

[4] Horizons Ephemeris System <horizons@ssd.jpl.nasa.gov>.

be seen from Figure 6 that the impact angles and speeds are highly dependent on the impact latitude on the Moon and hence warrant a more sophisticated approach to computing the secondary fluxes. It cannot be assumed that most impacts are at 45 degrees or are not highly oblique.

Other time frames may be simulated, such a week, a month, or a year, and can also vary as a function of time. In the current model output, a 19-year averaged flux is used.

3.1.1 Ephemeris Definition

3.1.2 Selenographic Extent

3.2 Sporadic Meteoroid Complex

3.2.1 Angular Distribution

3.2.2 Density Distribution

3.2.3 Mass Distribution

3.3 Near-Earth Objects

3.3.1 Speed Distribution

3.3.2 Mass Distribution

3.4 Meteoroid Showers

4 Secondary Flux Environment

4.1 Ejecta Distribution

4.1.1 Speed Distribution

4.1.2 Zenith Distribution

4.1.3 Azimuth Distribution

4.2 Mass/Particle Size Distribution

4.3 Orbital Mechanics

4.3.1 Crater on Surface to Observer at Surface

4.3.2 Crater on Surface to Observer at or above Surface

4.4 Selenographic Distance & Bearing

5 Scaling Laws

5.1 Crater Size – Strength & Gravity Regime

5.2 Minimum & Maximum Ejected Speed

5.3 Maximum Ejected Particle Mass

5.4 Mass Ejected from Crater

References

Carrier, W. D., Lunar soil grain size distribution, *The moon*, *6*(3-4), 250–263, 1973.

Carrier III, W. D., Particle size distribution of lunar soil, *Journal of Geotechnical and Geoenvironmental Engineering*, *129*(10), 956–959, 2003.

Heiken, G. H., D. T. Vaniman, and B. M. French, *Lunar Sourcebook, a user's guide to the Moon*, Cambridge University Press, 1991.

Housen, K. R., and K. A. Holsapple, Ejecta from impact craters, *Icarus*, *211*(1), 856–875, 2011.

Koschny, D., and E. Grün, Impacts into ice–silicate mixtures: Ejecta mass and size distributions, *Icarus*, *154*(2), 402–411, 2001.

Singer, K. N., B. L. Jolliff, and W. B. McKinnon, Lunar secondary craters and estimated ejecta block sizes reveal a scale-dependent fragmentation trend, *Journal of Geophysical Research: Planets*, *125*(8), e2019JE006,313, 2020.

Slyuta, E., Physical and mechanical properties of the lunar soil (a review), *Solar System Research*, *48*(5), 330–353, 2014.